Asian Journal of Chemistry; Vol. 38, No. 5 (2026), 1221-1233
ASIAN JOURNAL OF CHEMISTRY
https://doi.org/10.14233/ajchem.2026.35595

Electrochemical Sensor Based on an Acetylene Black Nanoparticles Pencil Graphite Composite for Trace Determination of Avanafil and its Interaction with Doxazosin Drug

MOHAMED IBRAHIM*, YASSIEN TEMERK*, HOSSIENY IBRAHIM, MOHAMED KOTB and MOHAMED SALAH

Chemistry Department, Faculty of Science, Assiut University, Assiut 71516, Egypt

*Corresponding authors: E-mail: msayed217@aun.edu.eg; temerk@aun.edu.eg

Received: 11 January 2026 *Accepted*: 21 March 2026 *Published online*: 4 May 2026 AJC-22347

Avanafil (AVA), a phosphodiesterase inhibitor effective in treating erectile dysfunction, can be rapidly and sensitively detected through cost-efficient electrochemical techniques. In this study, a novel voltammetric sensor based on a composite pencil graphite paste electrode (CPG-PE) improved with acetylene black nanoparticles (ABNPs/CPG-PE) for the trace quantification of AVA in the pharmaceutical formulations and biological fluids. The ABNPs/CPG-PE displayed high efficiency in oxidation of AVA employing adsorptive stripping square-wave voltammetry (AdS-SWV) in phosphate buffer (pH 7.0). AdS-SWV was effectively utilised for AVA detection using ABNPs/CPG-PE as a selective and sensitive method demonstrating two distinct linear concentration ranges of 0.002-1.96 μM and 1.96-19.6 μM AVA. The LOD and LOQ were 9.3×10^{-10} M and 3.1×10^{-9} M, respectively, with a sensitivity of 59.97 μA μM^{-1} cm^{-2}. Furthermore, the electrochemical behaviour of AVA in the presence of antihypertensive doxazosin (DOX) as a selective α-blocker on ABNPs/CPG-PE was explored and the interaction between AVA and DOX drugs was discussed.

Keywords: Avanafil, Electrochemical sensor, Acetylene black, Pharmaceutical analysis, Doxazosin drug, Drug-drug interactions.

INTRODUCTION

Avanafil (AVA) distinguishes itself as a phosphodiesterase-5 (PDE-5) inhibitor, marking the most recent inclusion in this class of medications. It offers greater selectivity and faster onset of action when contrasted with other PDE-5 inhibitors [1-4]. The use of AVA drug requires careful monitoring particularly when co-administered with medication that interact with it. In this regard, co-administration of AVA drug with antihypertensive α1-blockers such as doxazosin (DOX) causes a profound decline in blood pressure or diverse effects. Consequently, there is a critical need to investigate the effects of antihypertensive drug DOX on the erectile dysfunction drug AVA to determine the potential of drug-drug interactions and assess whether dose adjustments of AVA are warranted [5,6]. Hence, stringent quality control of AVA is imperative to ensure the efficacy and appropriate dosing in patients.

As of now, a few analytical methods have been employed to detect AVA in its dosage forms and biological fluids, including spectrofluorimetry [7,8], spectrophotometry [9], thin layer chromatography [10], liquid chromatography-mass spectrometry (LC-MS) [11]. Furthermore, stability-indicating liquid chromatography with diode array detection and liquid chromatography coupled with mass spectrometry methods were applied to measure the concentration of AVA in its pharmaceutical formulations [12]. Although most of these methods are efficient and accurate in determining the target drug, they are often costly and involve complex analysis procedures. In recent years, electrochemical methods offer simplicity, cost-effectiveness, sensitivity and swift operational performance, underscoring a variety of advantages. A review of the literature on AVA revealed that only a small number of studies have addressed the electrochemical detection of AVA, employing modified electrodes [13-15]. For the quick assessment of numerous drugs, electroanalytical techniques like square wave voltammetry (SWV) have been used [16-18]. Moreover, the use of appropriate nanomaterials for modifying surfaces can notably improve analytical capabilities such as selectivity, sensitivity, precision and long-term stability.

In the field of electroanalytical investigation, many endeavors have been made to advance modified electrodes through a range of nanomaterials and nanostructures [19-23]. Various nanomaterials have been employed to modify electrodes, aiming to broaden the linear range, enhance the select-

This is an open access journal and articles are distributed under the terms of the Attribution 4.0 International (CC BY 4.0) License. This license lets others distribute, remix, tweak and build upon your work, even commercially, as long as they credit the author for the original creation. You must give appropriate credit, provide a link to the license and indicate if changes were made.

ivity and boost the detection limit for detecting numerous compounds [24-26]. Consequently, there remains a need to develop a sensitive, simple and rapid analytical method to detect AVA and explore its interaction with the antihypertensive drug DOX.

Lately, there has been notable attention concerning electrochemical sensors using acetylene black nanoparticles (ABNPs). ABNPs, a special form of carbon black with a porous structure, exhibits remarkable properties including superior electrical conductivity, extensive surface area, strong adsorption capacity, small particle size, a highly branched chain structure, as well as excellent chemical stability [27]. The acetylene black based composites exhibited a hydrophilic surface characterised by a significant level of structural defects linked to the intrinsic functionalisation of ABNPs. In contrast, the graphite-based composites displayed a more hydrophobic nature due to the lower degree of functionalisation in graphite [28]. Furthermore, the electrodes derived from ABNPs demonstrated more homogeneous surfaces with reduced roughness compared to those made from graphite, indicating greater cohesion and spreadability attributed to the nanometric properties of ABNPs. As a result, the ABNPs displays significant potential for use as an electric transducer in a wide range of sensing applications. This capability is further enhanced through surface modifications with nanomaterials, which increase the active surface area and catalytic activity, thereby improving the conductivity of the modified electrode. On the other hand, pencil graphite lead has acquired great attention in electrochemistry due to its excellent electrical conductivity, cost-effective production and physical robustness. Electrochemical sensors modified with ABNPs show great potential for enhancing sensitivity and lowering detection limits in various analyses [29-33]. To enhance the electrocatalytic activity of pencil graphite lead, we propose a novel electrochemical sensor employing a composite pencil graphite paste electrode (CPG-PE) incorporated with ABNPs.

The objective of the present work is to fabricate a new electrochemical sensor platform based on a composite pencil graphite paste electrode (CPG-PE) improved with acetylene black nanoparticles (ABNPs/CPG-PE) for the trace determination of AVA in pharmaceutical formulations and biological fluids using adsorptive stripping square wave voltammetry (AdS-SWV). Moreover, the proposed sensor (ABNPs/CPG-PE) is also applied to investigate the interaction between the antihypertensive drug doxazosin (DOX), a selective alpha blocker and AVA. The understanding of potential drug-drug interaction is crucial for preventing severe side effects in patients.

EXPERIMENTAL

Avanafil (AVA) was kindly supplied as a gift from NODCAR, El-Dokki, Giza, Egypt. Acetylene black (AB, carbon black, acetylene, 50% compressed, 99.9+%, average particle size 42 nm) and paraffin oil were obtained from Alfa Aesar. The pencil graphite was available as pencil lead from HB Prima. To prepare the stock solution (1×10^{-3} M), ethanol was mixed with the appropriate amounts of AVA. As electrolytes Britton–Robinson buffer (BRB), McIlvaine buffer (MB) and phosphate buffer were used. The morphology of both CPG and the ABNPs/CPG nanocomposite was characterized using scanning electron microscopy (SEM). All the electrochemical measurements [CV, adsorptive stripping square-wave voltammetry (AdS-SWV) and EIS] were performed using an EG&G 263A Potentiostat/galvanostat and CS100E portable potentiostat. A three-electrode system was used for the voltammetric detection of AVA. A Ag/AgCl/saturated KCl electrode was used as a reference electrode and a platinum wire was used as counter electrode.

Electrochemical procedure: The voltammetric response of AVA at modified and unmodified electrodes was investigated in PBS pH 7.0. A suitable volume of AVA solution was added by a micropipette to the electrochemical cell containing 5 mL PBS pH 7.0. For AdAS-SWV experiments, 0.2 V was selected as accumulation potential (E_{acc}) and 120 s as the accumulation time (t_{acc}). The stirrer was turned off at the end of accumulation time and the solution was allowed to settle for 15 s before the voltammetric scan. The AdAS-SWV measurements were performed using a step height of 10 mV, a frequency of 100 Hz and a pulse height of 8 mV.

Preparation of real samples: Urine and serum samples of healthy volunteers were collected and stored frozen. Urine samples were centrifuged and filtered before use. A 1 mL urine sample was diluted with PBS pH 7.0 to a predefined volume and no pre-treatment was done. A 0.2 mL aliquot of the serum sample was treated with 2 mL methanol as a serum protein precipitating agent. The precipitated proteins were separated by centrifugation for 20 min at 4000 rpm. Each sample was diluted 10 times with PBS pH 7.0 before measurement. After preparing the sample, it was transferred to an electrochemical cell for analysis.

The pharmaceutical sample (Atconafil 200 mg, Atco Pharma) was procured from the local drug store. Five tablets were precisely measured, crushed into a homogenized fine powder and dissolved in ethanol. The solution was sonicated for 20 min in an ultrasonic bath for complete homogenisation. The obtained solution was filtered using Whatman filter paper and diluted with PBS pH 7.0 to achieve the required concentration.

VRE-Doxazosin interaction procedure: To prepare a stock solution of doxazosin, 5 tablets of Dosin 1 mg (Egyptian International Pharmaceutical Industries Company - EIPICO) were finely ground and an accurately weighed portion of the powdered tablets was dissolved in 5 mL of ethanol. To assess the response, a known volume of AVA was added to 5 mL of PBS of pH 7.0. The response was measured after each successive addition of doxazosin stock solution. The interaction between doxazosin and AVA was subsequently studied at various temperatures.

Preparation of the electrodes: Composite pencil graphite (CPG) powder was derived from HB-type composite pencil graphite leads (CPGLs) sourced from Prima, utilizing a ball mill grinding machine. The bare composite pencil graphite paste electrode (CPG-PE) was obtained by mixing CPG and paraffin oil in an agate mortar (80:20 w/w). The resulting paste was inserted into a Teflon tube with a geometric area of 0.07 cm^2. Subsequently, the surface was smoothed by polishing it with a piece of paper. The ABNPs-modified CPG-PEs (ABNPs/CPG-PE) were prepared by mixing ABNPs (4.2, 7.3 and 10.4%) with CPG and 20% paraffin oil until well blended.

RESULTS AND DISCUSSION

Morphological studies: SEM provides high-resolution characterisation of surface morphology in both CPG and ABNPs/CPG, providing detailed insights into topography, texture and shape. With its superior magnification and resolution, SEM enables visualization of fine surface features and microstructural characteristics at the nanoscale. Fig. 1a-c displays SEM images of both CPG and ABNPs/CPG. The CPG structure appears flat, while the AB-modified CPG exhibits a clustered surface with white patches, indicating the modification of the CPG surface with ABNPs.

Electrochemical studies of modified electrodes: The electrochemical properties of the prepared electrodes, particularly CPG-PE and ABNPs/CPG-PE, were investigated in the presence of $[Fe(CN)_6]^{3-/4-}$ using cyclic voltammetry (CV) at 100 mV s^{-1} as shown in Fig. 2a. The CVs show a peak-to-peak separation (ΔE_P) of 163 mV for CPG-PE and 129 mV for ABNPs/CPG-PE. $[Fe(CN)_6]^{3-/4-}$ exhibited a higher anodic peak current (163.3 ± 3.8 μA, RSD = 2.3%) on ABNPs/CPG-PE compared to the unmodified CPG-PE (130.3 ± 4.4 μA, RSD = 3.4%). The findings suggest that ABNPs can potentially augment the conductivity and surface area of the electrode as well as improve the reversibility of electron transfer processes.

Electrochemical impedance spectroscopy (EIS) measurements were performed in the presence of $[Fe(CN)_6]^{3-/4-}$ to further elucidate the surface characteristics of the modified electrodes. Fig. 2b shows the Nyquist plots for the unmodified CPG-PE and the ABNPs/CPG-PE. The unmodified CPG-PE exhibited a higher charge transfer resistance (R_{ct}) of 1737 ± 45 Ω, RSD = 2.6%, indicating significant electron transfer resistance to the redox probe. With the incorporation of ABNPs into the CPG-PE, R_{ct} decreased to 891 ± 26 Ω, RSD = 2.9%, suggesting that the hybrid composite ABNPs/CPG-PE enhanced the electron transfer process potentially due to its excellent conductivity. The agreement between the EIS data and the CV confirmed the improved properties of ABNPs/CPG-PE as basis for the envisioned electrochemical sensor.

To investigate the effective surface areas of ABNPs/CPG-PE and the bare CPG-PE, the influence of the scan rate on the CV response of the redox couple $[Fe(CN)_6]^{3-/4-}$ were measured (Fig. 3). Using the Randles-Sevcik equation, $I_{Pa} = (2.69 \times 10^5)\, n^{3/2} A D^{1/2} \nu^{1/2} C$ (I_{Pa}: anodic peak current value; A: the active electrode area; n: number of electrons; C: the concentration of $[Fe(CN)_6]^{3-/4-}$; ν: scan rate; and D: diffusion coefficient) [34], the effective surface areas of the bare CPG-PE and ABNPs/CPG-PE electrodes were determined to be 0.06 ± 0.001 cm^2, RSD = 1.7% and 0.12 ± 0.003 cm^2, RSD = 2.5%, respectively (Fig. 2c). The increased electroactive surface

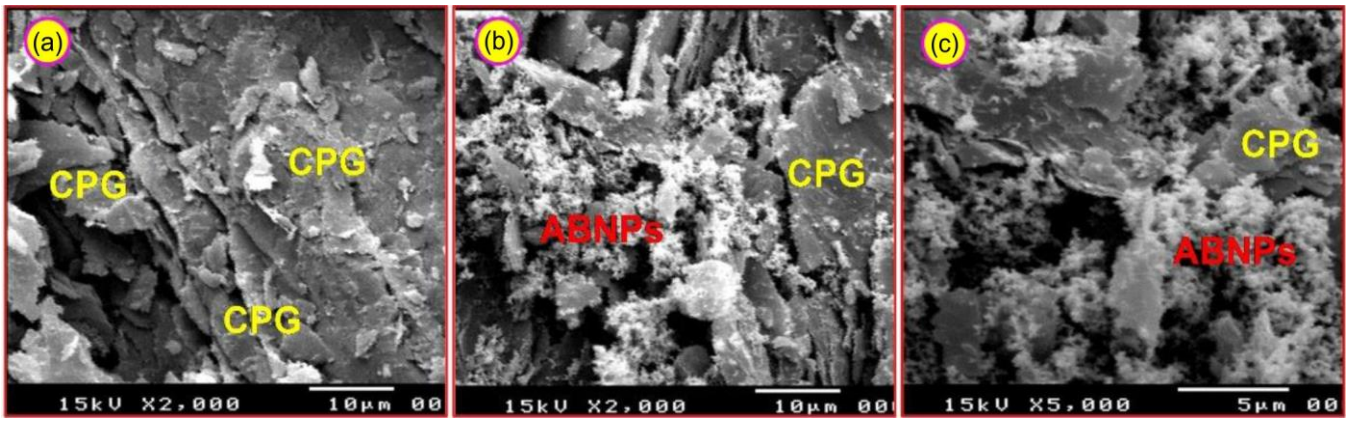

Fig. 1. SEM images of CPG (a) and ABNPs/CPG hybrid composite (b & c) at low and high magnification

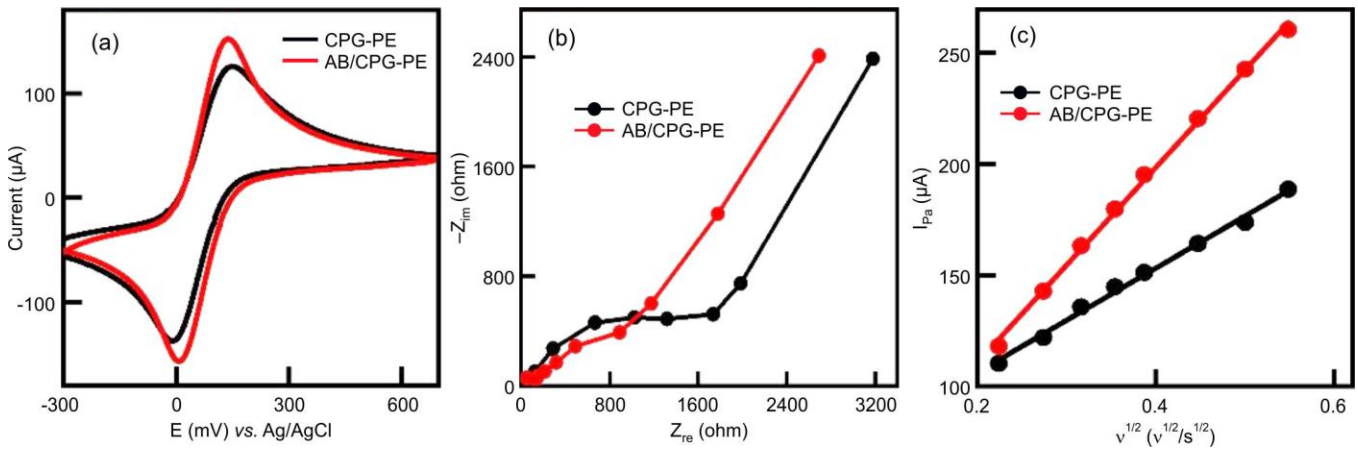

Fig. 2. (a) CVs and (b) Nyquist plots of CPG-PE and AB/CPG-PE in 5 mM $[Fe(CN)_6]^{3-}/[Fe(CN)_6]^{4-}$ (1:1 mixture) solution containing 0.1 M KCl at a scan rate of 100 mV s^{-1}, (c) Plot of I_{pa} *vs.* $\nu^{1/2}$

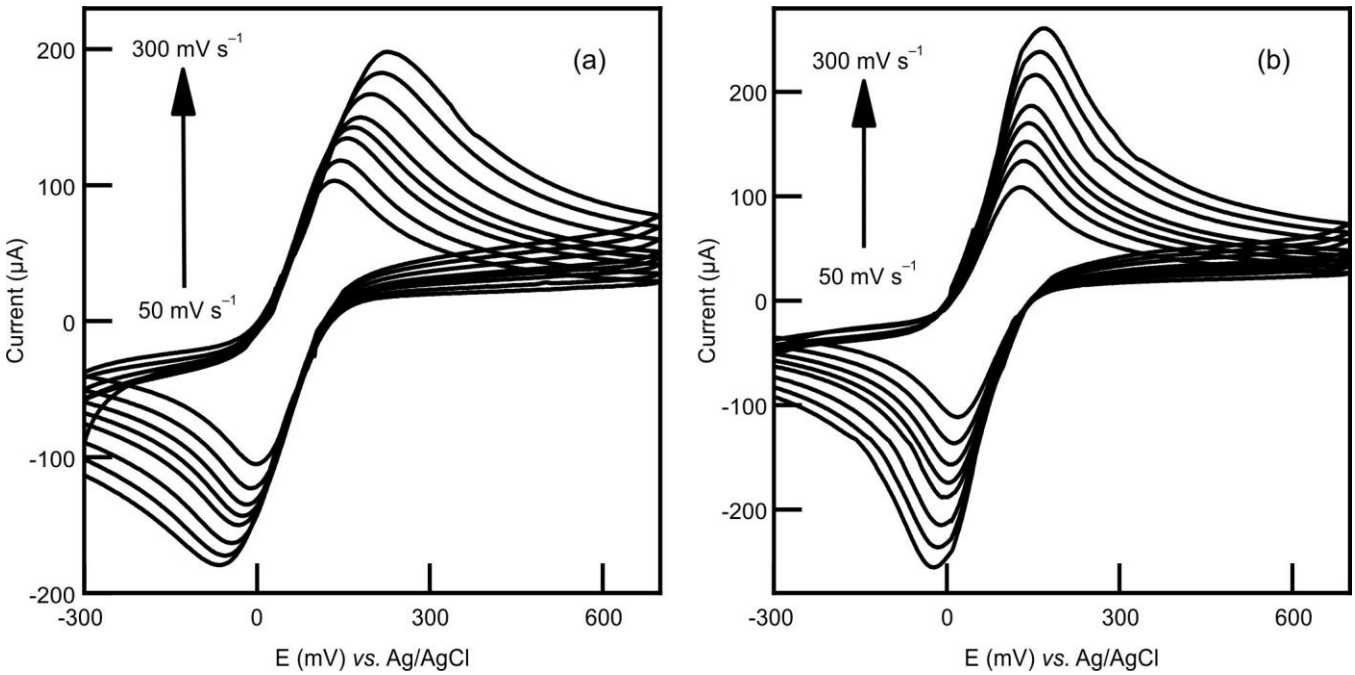

Fig. 3. CVs of (a) bare CPG-PE and (b) ABNPs/CPG-PE in 5 mM $[Fe(CN)6]^{3-/4-}$ at different scan rates (50-300 mV s^{-1})

area of the modified electrode reflects the role of ABNPs as an effective enhancer, offering a larger surface and promoting electron transfer across the interface.

Electrochemical behaviour of AVA at AB/CPG-PE: Fig. 4a shows the CVs obtained at a concentration of 38.4 μM AVA at both the unmodified CPG-PE and the ABNPs/CPG-PE in PBS pH 7.0. AVA displayed a single irreversible oxidation peak at both electrodes, attributed to a one proton, two-electron oxidation process in the forward scan, with no reduction peaks observed during the reverse scan, confirming the irreversibility of the oxidation process. Compared to the unmodified CPG-PE (3.88 ± 0.058 μA, RSD = 1.5%), a significant increase in the anodic current was observed for the ABNPs/CPG-PE (5.27 ± 0.1 μA, RSD = 1.9%). This highlights that the presence of ABNPs enhances conductivity, increases surface area and facilitates electron transfer between AVA and the ABNPs/CPG-PE surface. Consequently, the sensitivity of AVA detection is markedly improved when using the ABNPs film-modified CPG-PE.

The oxidation behaviour of AVA was also investigated using AdS-SWV in PBS (Fig. 4b). The electrochemical response of 19.6 μM AVA at ABNPs/CPG-PE is more sensitive when using AdS-SWV compared to CV, as this technique enhances analytical signals by eliminating the non-faradaic currents that occur with CV. In this context, the anodic peak current at the ABNPs/CPG-PE was 28.35 ± 0.65 μA, RSD = 2.3%, which is considerably higher than the current response obtained through CV as well as compared to that attained at the unmodified CPG-PE (19 ± 0.55 μA, RSD = 2.9%). The substantial increase in the anodic peak current provides evidence of a catalytic effect of ABNPs in CPG-PE and an enhanced electrode area. The quantity of ABNPs can influ-

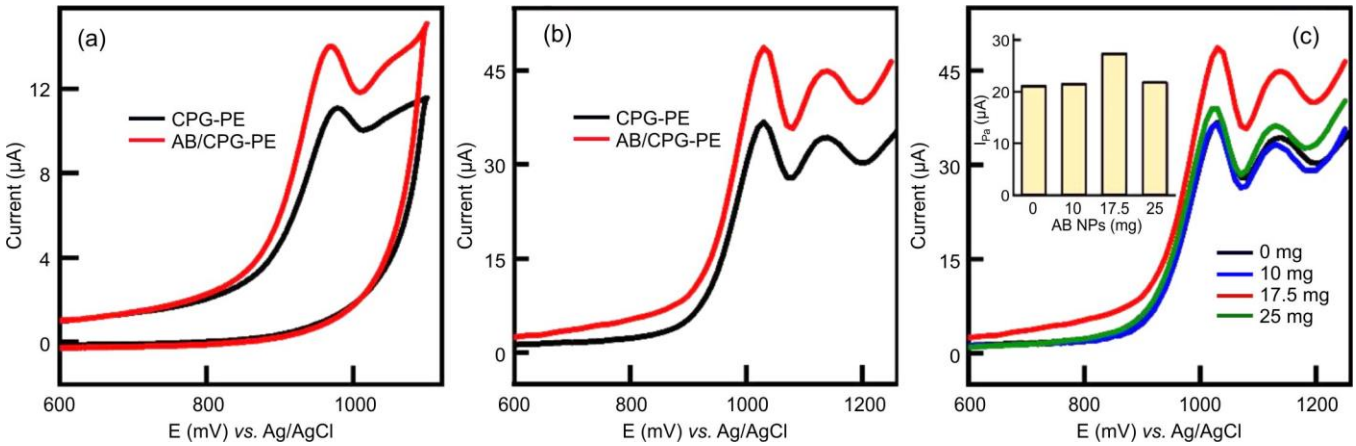

Fig. 4. (a) CVs of 38.5 μM AVA and (b) AdS-SW voltammograms of 19.6 μM AVA in PBS of pH 7.0 obtained for bare CPG-PE and AB/CPG-PE at a scan rate of 100 mV s^{-1}; (c) AdS-SW voltammograms of 19.6 μM AVA in PBS of pH 7.0 at CPG-PE modified with different amounts of ABNPs. Inset: The bar diagram exhibits the effect of different amounts of AB on the anodic peak response

ence the electrochemical behaviour of AVA at ABNPs/CPG-PE and hence the optimal amount of ABNPs in the CPG paste was investigated. Fig. 4c illustrates the impact of the quantity of ABNPs on the oxidation peak current of AVA during AdS-SWV. Three distinct modified electrodes were examined maintaining consistent conditions and varying the ABNPs amount from 10 to 25 mg. With increasing amount of ABNPs the AVA oxidation peak current gradually rose reaching its maximum at 17.5 mg ABNPs most likely due to an enhanced surface area. The peak current of AVA slowly decreased as the ABNPs quantity increased further.

Influence of pH and supporting electrolyte: The effect of solution pH, ranging from 3.0 to 8.0, on the electrochemical oxidation of 19.6 μM AVA at ABNPs/CPG-PE was studied in PBS employing AdS-SWV (Fig. 5a). As depicted in Fig. 5b, the peak current of AVA is modulated by changes in pH value, peaking at pH 7.0. Thus, all subsequent experiments were conducted in pH 7.0 PBS to achieve optimal sensitivity for AVA determination. The dependence of peak potential (E_{pa}) on pH was investigated, revealing a linear relationship. The peak potential was observed to shift negatively with increasing pH, indicating that protons are involved in the oxidation process. The equation for this relationship is E_p(V) = 1.271 - 0.030 pH (R^2 = 0.991). A slope of 0.030 V pH^{-1} indicates that the electrochemical reaction of AVA at ABNPs/CPG-PE involves one proton and two electrons in the oxidation mechanism (**Scheme-I**) [34]. The influence of different electrolytes on the AVA oxidation current at ABNPs/CPG-PE was studied using phosphate buffer, Britton–Robinson (PBS) and McIlvaine buffer (Fig. 5c). The peak height achieved a maximum and the curve shape was more symmetric in PBS at pH 7.0 compared to the other electrolytes. Thus, PBS with pH 7.0 was selected for the subsequent voltammetric experiments.

Influence of potential scan rate: The kinetic characteristics of the developed electrode and the mechanism of the electrooxidation process of AVA at the electrode surface can be determined by examining the influence of scan rate (ν) on the voltammetric response of AVA. The CVs of AVA at ABNPs/CPG-PE were analysed with the scan rate increasing from 25 to 300 mV s^{-1} in PBS of pH 7.0 (Fig. 6a). The anodic shift of the oxidation peak potential with increasing scan rate suggests a quasi-reversible or irreversible electrochemical process [35,36]. The peak current increases with ν represented by the equation: I_{pa} (μA) = 0.285 + 0.0296 V (mV s^{-1}) (R^2 = 0.997), suggesting that the electrooxidation mechanism of AVA at ABNPs/CPG-PE is governed by a kinetic adsorption process (Fig. 6b). This is more confirmed by plotting the log I_p against the log ν (Fig. 6c), resulting in a linear relationship: log I_{pa} (μA) = 0.951 log ν (mV s^{-1}) – 1.39 (R^2 = 0.998). The slope of 0.951 confirms that the irreversible electrode process of AVA at ABNPs/CPG-PE is controlled by the adsorption of AVA (for a pure adsorption process, the slope equals 1) [37]. A linear relationship between the E_{pa} and ln ν was established as [E_{pa} (V) = 0.78471 + 0.03028 ln ν (mV s^{-1}) (R^2 = 0.985)] for CPG-PE and [E_{pa} (V) = 0.8266 + 0.02988 ln ν (mV s^{-1}) (R^2 = 0.991)] for ABNPs/CPG-PE (Fig. 6d). Following the Laviron theory for an electrode process that is entirely irreversible and controlled by adsorption [38], E_p is expressed as:

$$E_p = E^0 - \left(\frac{RT}{\alpha nF}\right)\ln\left(\frac{RTk_s}{\alpha nF}\right) + \left(\frac{RT}{\alpha nF}\right)\ln \nu \qquad (1)$$

According to the Laviron equation and the slope obtained from the previous equation [E_{pa} (V) = 0.8266 + 0.02988 ln ν (mV s^{-1}) (R^2 = 0.991)] for ABNPs/CPG-PE, the value of αn can be calculated as following: [Slope = 0.02988 = (RT/αnF)]. Where α represents the electron transfer coefficient and n denotes the number of electrons transferred, while R and T retain their conventional meanings. The calculated value of αn was approximately 0.86. Since, the electrooxidation process of AVA was found to be completely irreversible, α was assumed to be 0.5 [34]. Therefore, the number of electrons transferred (n) was determined to be 1.72, which is approximately equal to 2 [13]. These results further affirm that the electrooxidation process of AVA at the ABNPs/CPG-PE involves the consumption of two electrons and one proton. The detailed pathway of AVA oxidation is illustrated in **Scheme-I**.

Furthermore, the charge transfer rate constant (k_s) value can be deduced from the intercept of the preceding plot if the values of αn and E^0 are provided. The E^0 values are 0.86 V for CPG-PE and 0.92 V for ABNPs/CPG-PE by extrapolating the line to ν = 0 V s^{-1} on the ordinate of the E_p *vs.* ν plot.

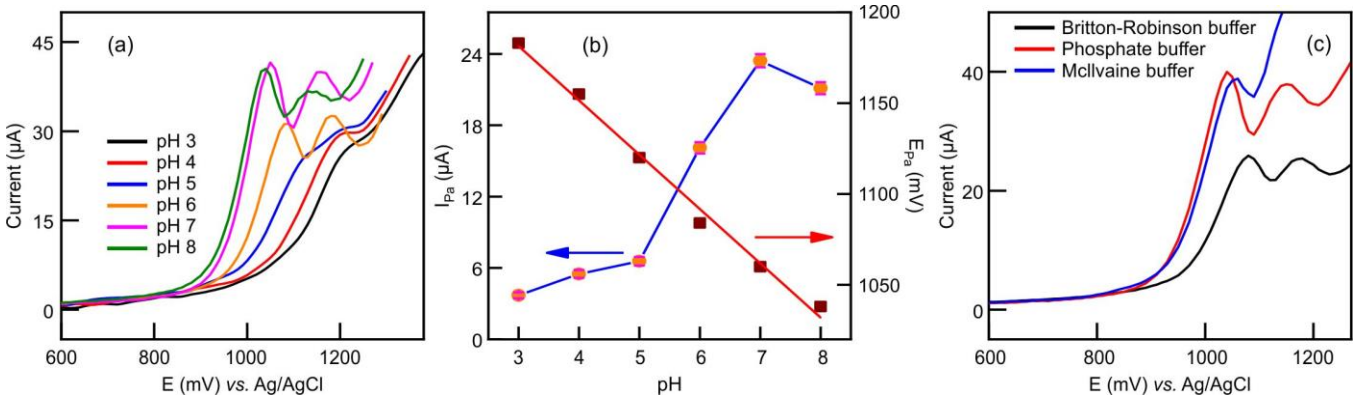

Fig. 5. (a) AdS-SW voltammograms of 19.6 μM AVA using an ABNPs/CPG-PE at different pH values (PBS); (b) Effect of pH on I_{pa} (■) and E_{pa} (●) at ABNPs/CPG-PE; (c) AdS-SW voltammograms of 19.6 μM AVA in different buffers of pH 7.0 obtained at ABNPs/CPG-PE

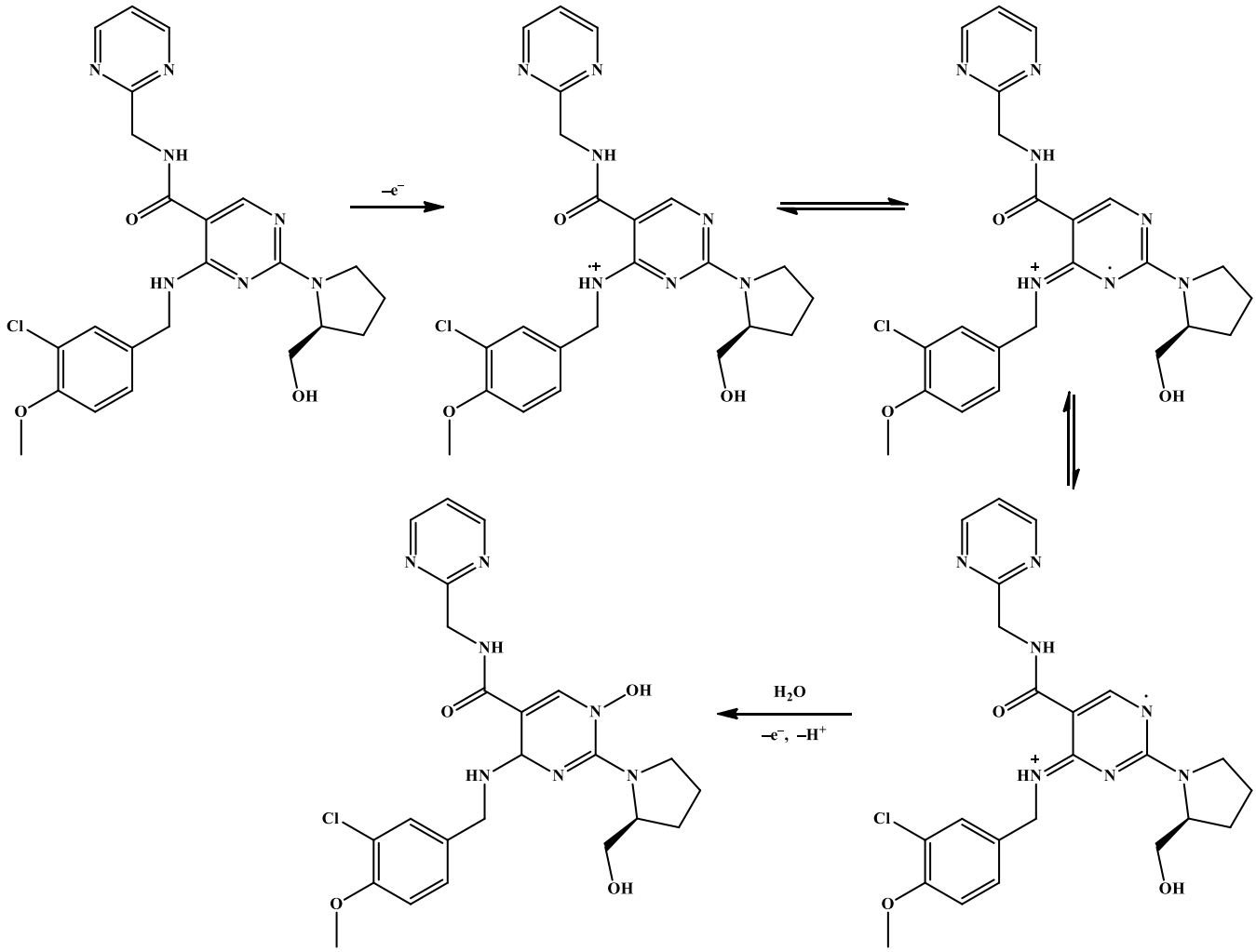

Scheme-I: Proposed electrochemical oxidation mechanism of AVA at ABNPs/CPG-PE sensing platform

Utilizing this data and eqn. 1, the derived k_s values were 397 and 762 s^{-1} for CPG-PE and ABNPs/CPG-PE, respectively. This may be due to the increased electrode surface area and enhanced electrical conductivity facilitated by ABNPs, suggesting a fast electron transfer process between the adsorbed AVA molecules and ABNPs/CPG-PE.

The amount of electroactive AVA (Γ, mol cm^{-2}) adsorbed on the surface of ABNPs/CPG-PE and bare CPG-PE was calculated using the following relationship [39]: Γ = Q/nFA, where Q is the charge involved in the oxidation process, F is the Faraday constant, n is the number of electrons (n = 2) and A is the area of the working electrode. The Γ values on the ABNPs/CPG-PE and the bare CPG-PE were 2.43×10^{-9} and 1.99×10^{-9} mol cm^{-2}, respectively. The substantial increase in Γ for ABNPs/CPG-PE compared to CPG-PE suggests that ABNPs offers a significantly larger surface area and strongly influences the adsorption characteristics of AVA.

Parameters optimization: The optimizing measurement parameters such as frequency (*f*) and pulse height (E_a) is essential to enhance the AdS-SWV response for accurate AVA detection. Fig. 7a Illustrates the influence of E_a (ranging from 2 to 10 mV_{pp}) on the AdS-SWV of AVA, employing a frequency of 100 Hz, a 60 s accumulation time and a 10 mV scan increment. The peak current obtained at a pulse height of 8 mV_{pp} was the highest and was utilised for further experiments. Similarly, the effect of the frequency in the range from 20 to 100 Hz, the accumulation potential (E_{acc}) and accumulation time (t_{acc}) of AVA were investigated (Fig. 7b-d). The optimal conditions for high sensitivity and the best peak morphology were E_a = 8 mV_{pp}, *f* = 100 Hz, E_s = 10 mV, t_{acc} = 120 s and E_{acc} = 0.2 V.

Quantification of AVA at ABNPs/CPG-PE: The AdS-SWV in PBS pH 7.0 was used for AVA detection at ABNPs/CPG-PE, employing the optimised parameters derived above (Fig. 8a). Fig. 8b illustrates the calibration curve of AVA, featuring two distinct linear sections with different slopes. This indicates a correlation between the peak current and two separate ranges of AVA concentration. The initial linear section correlates with AVA concentrations ranging from 0.002-1.96 μM (I_{pa} (μA) = 4.198 (μM) [AVA] + 0.2752, R^2 = 0.997), while the second linear section relates to AVA concentrations from 1.96-19.6 μM (I_{pa} (μA) =1.21 (μM) [AVA] + 6.02, R^2 = 0.996). By applying the equations LOD = 3s/b and LOQ = 10s/b, where s is the standard deviation of the intercept and b is the slope of the calibration plot, the limit of detection (LOD) and limit of quantification (LOQ) for AVA

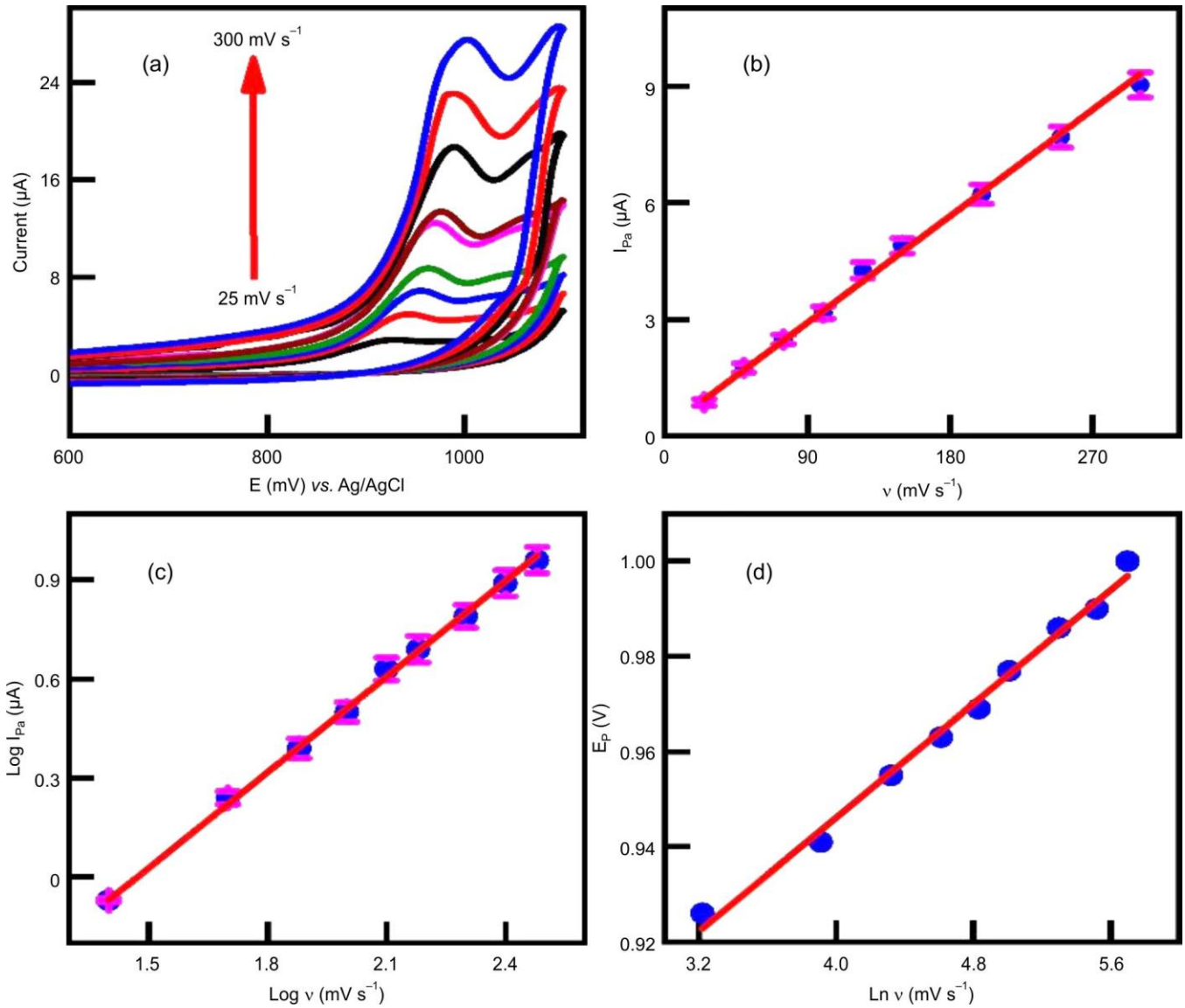

Fig. 6. (a) CVs of 38.5 μM AVA at an AB/CPG-PE at various scan rates in PBS (pH 7.0), (b) plot of I_{pa} (μA) *vs.* ν; (c) plot of log I_{pa} *vs.* log ν; (d) plot of E_{pa} (V) *vs.* ln ν. Error bars represent the standard deviation of triple measurements

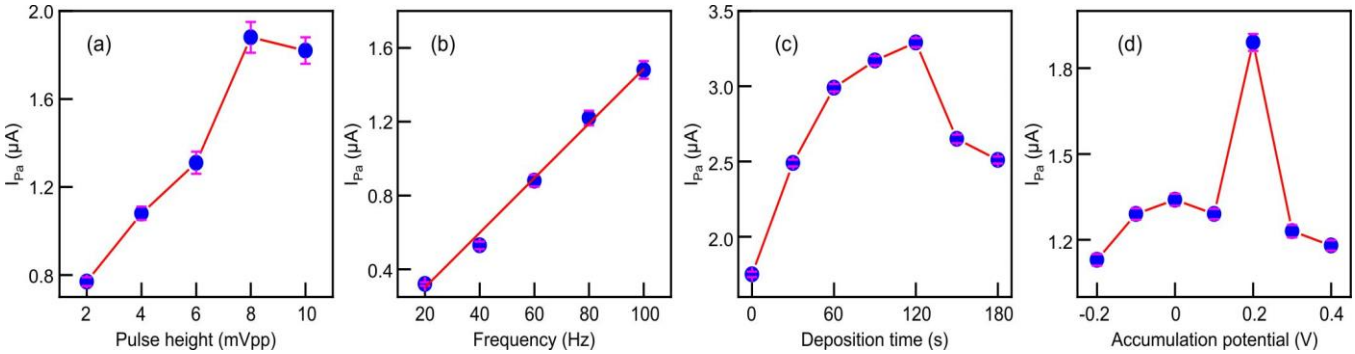

Fig. 7. Effects of (a) pulse height, (b) frequency, (c) accumulation time and (d) accumulation potential on the peak current of AVA. Error bar represents the standard deviation of triple measurements

within the lower range of concentration were calculated, with values of 9.3×10^{-10} M and 3.1×10^{-9} M (S/N = 3), respectively. The sensitivity of the AVA electrochemical sensor was evaluated to be 59.97 μA μM^{-1} cm^{-2}. The analytical results and the validation metrics for the proposed method were calculated and are summarised in Table-1.

The effectiveness of ABNPs/CPG-PE employed was compared with other studies utilizing various electrodes com-

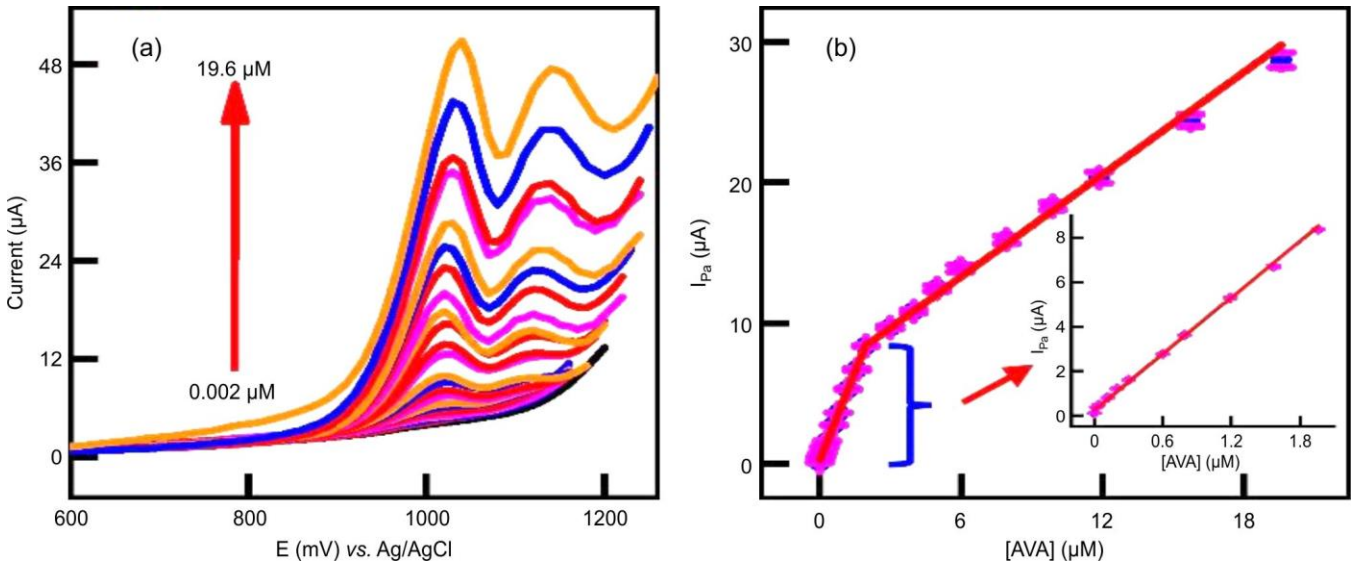

Fig. 8. (a) AdS-SW voltammograms for the determination of AVA over the concentration range of 2.0 nM to 19.6 µM at an ABNPs/CPG-PE electrode in phosphate-buffered saline (PBS) at pH 7.0; (b) corresponding calibration plot for AVA

TABLE-1
REGRESSION DATA OF THE CALIBRATION LINES FOR QUANTITATIVE DETERMINATION OF AVA IN BULK, SERUM AND URINE SAMPLES AT ABNPs/CPG-PE USING AdS-SWV

Parameters	Bulk	Serum	Urine
Linearity range (µM)	0.002-1.96	0.002-1.96	0.002-1.96
Slope (µA µM^{-1})	4.198	3.975	3.357
Standard error of slope	0.067	0.11248	0.04323
Intercept (µA)	0.2752	0.14299	0.1006
Standard error of intercept	0.022	0.02191	0.01033
Coefficient of determination (R^2)	0.997	0.9991	0.998
Number of measurements (n)	3	3	3
LOD (nM)	0.93	1.5	1.6
LOQ (nM)	3.1	5.0	5.4
Sensitivity (µA µM^{-1} cm^{-2})	59.97	56.79	47.96

prising primarily carbon-based materials for AVA determination (Table-2). ABNPs/CPG-PE reveals a wider linear range and a lower LOD. It was found that the LOD for AVA at ABNPs/CPG-PE was reduced by 76-, 40- and 38-fold compared to other carbon paste electrodes, namely ZnO-NPs/MWCNT/CPE, NiO-NPs/poly(sulf)/PGE and TiO_2/MWCNT/CPE, respectively (Table-2). The increased sensitivity and electrochemical efficacy of ABNPs-modified CPG-PE makes the proposed electrode superior in terms of activity for AVA oxidation when compared to carbon paste electrodes (CPE) modified with ZnO NPs and MWCNT (ZnO-NPs/MWCNT/CPE) [13], nanostructured NiO/sulphanilamide polymer film modified pencil graphite electrode (NiO-NPs/poly(sulph)/PGE) [14], CPE modified with TiO_2 NPs and MWCNT (TiO_2/MWCNT/CPE) [15]. The LOD and linear range (Table-2) also demonstrated superior results compared with spectrofluorimetry [7,8], spectrophotometry [9] and HPLC [10-12].

The electrochemical oxidation mechanism of AVA at ABNPs/CPG-PE was also compared with findings from other studies that employed different electrodes under varying solution conditions (Table-2). Based on the proposed oxidation mechanism, the oxidation of AVA at ABNPs/CPG-PE (pH 7.0) takes place at the secondary amino group producing a radical cation and involving the consumption of two electrons and one proton (**Scheme-I**). This mechanism closely resembles the electrochemical oxidation pathway of AVA at ZnO-NPs/MWCNT/CPE (pH 6) [13], occurring at the same secon-

TABLE-2
COMPARATIVE DATA OF THE PROPOSED ELECTROCHEMICAL SENSOR WITH OTHER REPORTED METHODS USED IN THE DETERMINATION OF AVANAFIL (AVA)

Methods	Modifier	pH	Linear range (µM)	LOD (nM)	Ref.
Spectrofluorimetry	–	–	0.1-3.70	21	[7]
Spectrofluorimetry	–	–	2.0-20.0	132	[8]
Spectrofluorimetry	–	–	20-310	48	[9]
HPTLC	–	–	1.0-10.0	141	[10]
LC-MS	–	–	0.1-6.6	–	[11]
LC-DAD	–	–	1.0-41.0	149	[12]
Voltammetry (SWV)	ZnO NPs/MWCNT/CPE	6.0	2.69-33.1	71	[13]
Voltammetry (SWV)	NiO NPs/Poly(sulf)/PGE	3.0	0.05-1.0	37	[14]
Voltammetry (SWV)	TiO_2/MWCNT/CPE	3.0	0.1-6.0	35	[15]
Voltammetry (AdS-SWV)	AB NPs/CPG-PE	7.0	0.002-1.96; 1.96-19.6	0.93	Present study

dary amino group and involving the transfer of two electrons and two protons. In contrast, at NiO-NPs/poly(sulf)/PGE (pH 3) [14] or TiO_2/MWCNT/CPE (pH 3) [15], the oxidation of AVA occurs at the nitrogen atom of the amide group, involving the transfer of one electron and one proton, followed by hydrolysis and cleavage of the amidic bond. These findings demonstrate that the electrochemical oxidation of AVA is influenced by the nanometric characteristics, the active surface sites and the catalytic properties of the modified electrode, as well as by the conditions of the solution.

Selectivity: The selectivity of the AdS-SWV method was investigated on the ABNPs/CPG-PE by studying the influence of various interfering substances on the detection of AVA. The results indicated that the presence of 10- or 50-fold concentrations of common interferents, such as ascorbic acid, uric acid, dopamine, glucose, mannitol and metal ions Mg^{2+} and K^+, did not significantly interfere with the AdS-SWV response of 8.0×10^{-7} M AVA, resulting in only a minor change of 2 to 3% (Table-3). Moreover, average recoveries ranging from 96.2% to 98.1% were achieved, indicating that the ABNPs/CPG-PE exhibits excellent selectivity towards AVA detection even in the presence of different interfering substances commonly found in pharmaceutical formulations and clinical settings.

TABLE-3
INFLUENCE OF INTERFERENTS ON THE VOLTAMMETRIC RESPONSES OF 8×10^{-7} M AVA AT ABNPs/CPG-PE

Interferent	Folds	Concentration (μM)	Recovery (%)
Ascorbic acid	10	8.0	98.1
Uric acid	10	8.0	97.8
Dopamine	10	8.0	97.5
Glucose	50	40.0	96.2
Mannitol	50	40.0	97.8
Mg^{2+}	10	8.0	96.7
K^+	50	40.0	96.4

Stability and reproducibility of modified sensor: The modified ABNPs/CPG-PE sensor showed high stability, retaining 98.2% of its initial peak current response for 0.8 μM AVA using AdS-SWV after 42 days, with a RSD% of 1.38%. Reproducibility was also evaluated using five distinct modified sensors independently fabricated following the same method, resulting in a RSD of 1.98%, indicating high reproducibility of the ABNPs/CPG-PE. Accuracy and precision of the suggested method were evaluated by measuring three different concentrations of AVA of 0.04, 0.84 and 7.94 μM using AdS-SWV. This was done in five independent series on the same day (intra-day) and at the same levels on five different days (inter-day) with the results presented in Table-4. As shown in Table-4, the RSD values are very low (RSD% < 3.80) and the recovery of AVA is approximately equal to 100%, demonstrating good accuracy and precision.

Analytical applications of ABNPs-modified CPG-PE for AVA determination: To assess the reliability of the ABNPs/CPG-PE, the suitability of the proposed voltammetric method was tested using a commercially available pharmaceutical drug (Atconafil) labeled AVA 200 mg. As stated in the experimental section, the preparation of the sample solution from the Atconafil drug should fall within the range of the AVA calibration plot. AdS-SWV analysis was then carried out using ABNPs/CPG-PE, as depicted in Fig. 9. The standard addition method was applied to determine the AVA concentration in the Atconafil drug. The detected value was found to be 195 mg/tablet, with a recovery rate of 97.5% and an RSD was 3.4% (n = 3), demonstrating the precision of the proposed method. The proposed voltammetric method can effectively determine AVA in pharmaceutical products, with no interference from the drug excipients during analysis.

The newly proposed method was utilised to determine AVA levels spiked into human biological fluids (human blood serum and urine samples) assessing the applicability of ABNPs/CPG-PE for real sample analysis. Human biological fluids free from AVA concentrations were spiked with varying amounts of standard AVA solution for subsequent analysis under the optimum conditions and the calibration plots are shown in Fig. 10. As expected from the calibration graphs, two linear dynamic ranges of 0.002 to 1.96 μM AVA and 1.96 to 19.6 μM AVA were identified for both serum and urine samples, respectively. As presented in Table-4, the recoveries ranging from 97.6% to 105.0% indicate a promising potential of the new electrochemical ABNPs/CPG-PE sensor for AVA detection in biological samples.

TABLE-4
PRECISION (INTRA- AND INTER-DAY) AND ACCURACY FOR ASSAY OF AVA (n = 3)

Added (μM)	Inter-day				Intra-day			
	Found (μM)	RSD (%)	Recovery (%)	Bias (%)	Found (μM)	RSD (%)	Recovery (%)	Bias (%)
	Bulk form				Bulk form			
0.04	0.0397	3.80	99.25	0.75	0.042	3.76	105.00	-5.00
0.84	0.8370	2.46	99.64	0.36	0.842	2.63	100.24	-0.24
7.94	7.9900	1.94	100.63	-0.63	7.790	1.54	98.11	1.89
	Serum sample				Serum sample			
0.04	0.0404	3.43	101.00	-1.00	0.042	3.57	105.00	-5.00
0.84	0.8700	3.52	103.57	-3.57	0.880	2.55	104.76	-4.76
7.94	7.8600	1.73	98.99	1.01	7.942	2.25	100.03	-0.03
	Urine sample				Urine sample			
0.04	0.042	3.14	105.00	-5.00	0.041	3.78	102.50	-2.50
0.84	0.848	3.30	100.95	-0.95	0.820	3.88	97.62	2.38
7.94	7.900	1.60	99.50	0.50	7.980	1.59	100.50	-0.50

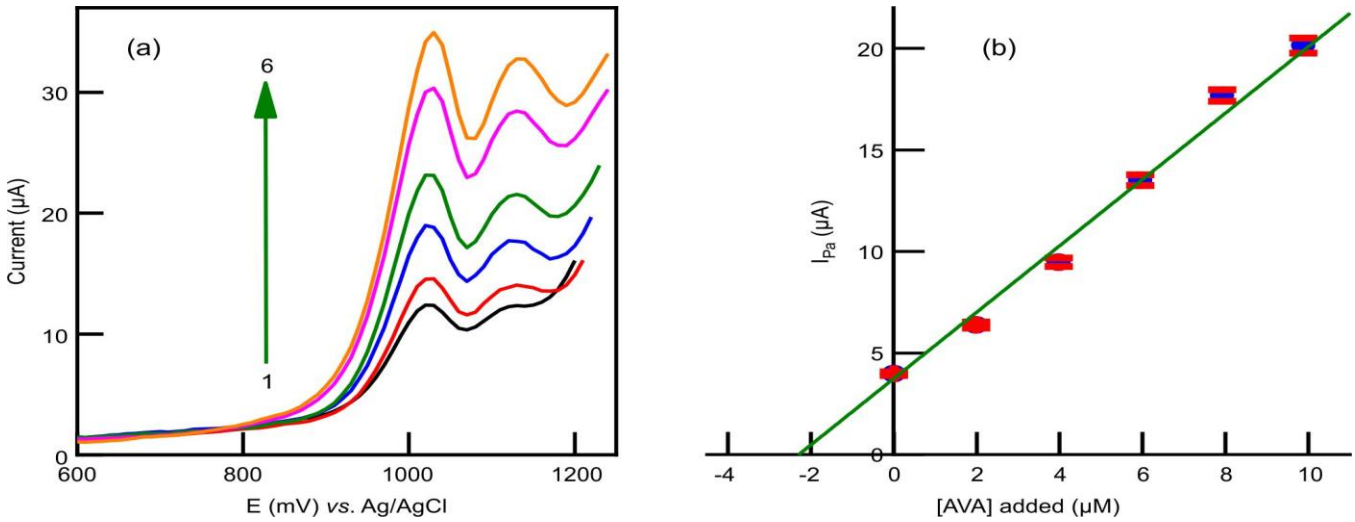

Fig. 9. (a) AdS-SW voltammograms of the diluted samples of AVA 200 mg; (b) corresponding linear calibration plots of peak current *vs.* concentration of added AVA. [Pulse height = 8 mV, frequency = 100 Hz, scan increment = 10 mV, accumulation potential = 0.2 V, accumulation time = 120 s]. Error bar represents the standard deviation of triple measurements

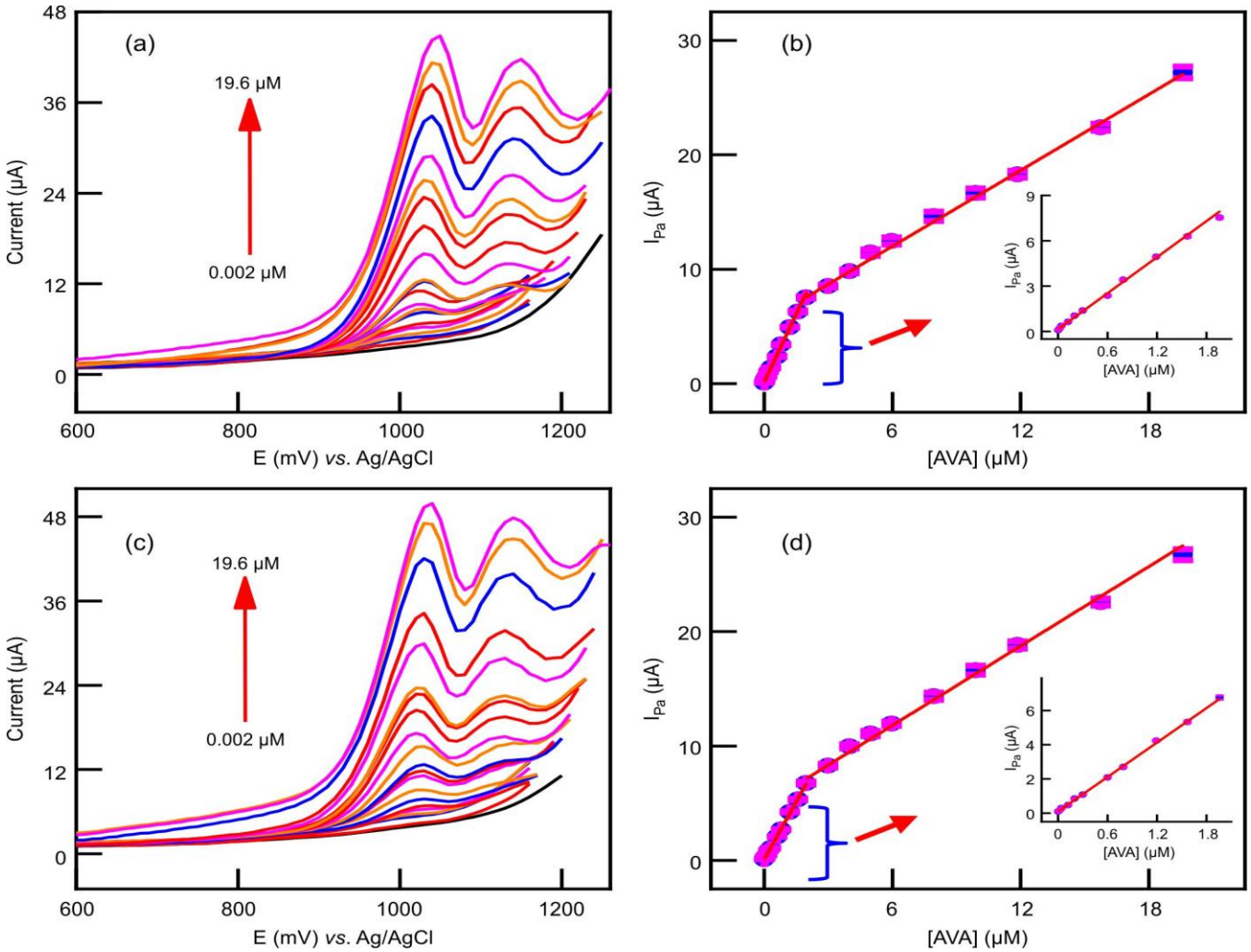

Fig. 10. (a) AdS-SW voltammograms for determination of AVA spiked human serum sample at ABNPs/CPG-PE in PBS (pH 7.0); (b) corresponding calibration plot for AVA; (c) AdS-SW voltammograms for determination of AVA spiked human urine sample at ABNPs/CPG-PE in PBS (pH 7.0); (d) corresponding calibration plot for AVA [Pulse height = 8 mV, frequency = 100 Hz, scan increment = 10 mV, accumulation potential = 0.2 V, accumulation time = 120 s]. The error bar represents the standard deviation of triple measurements

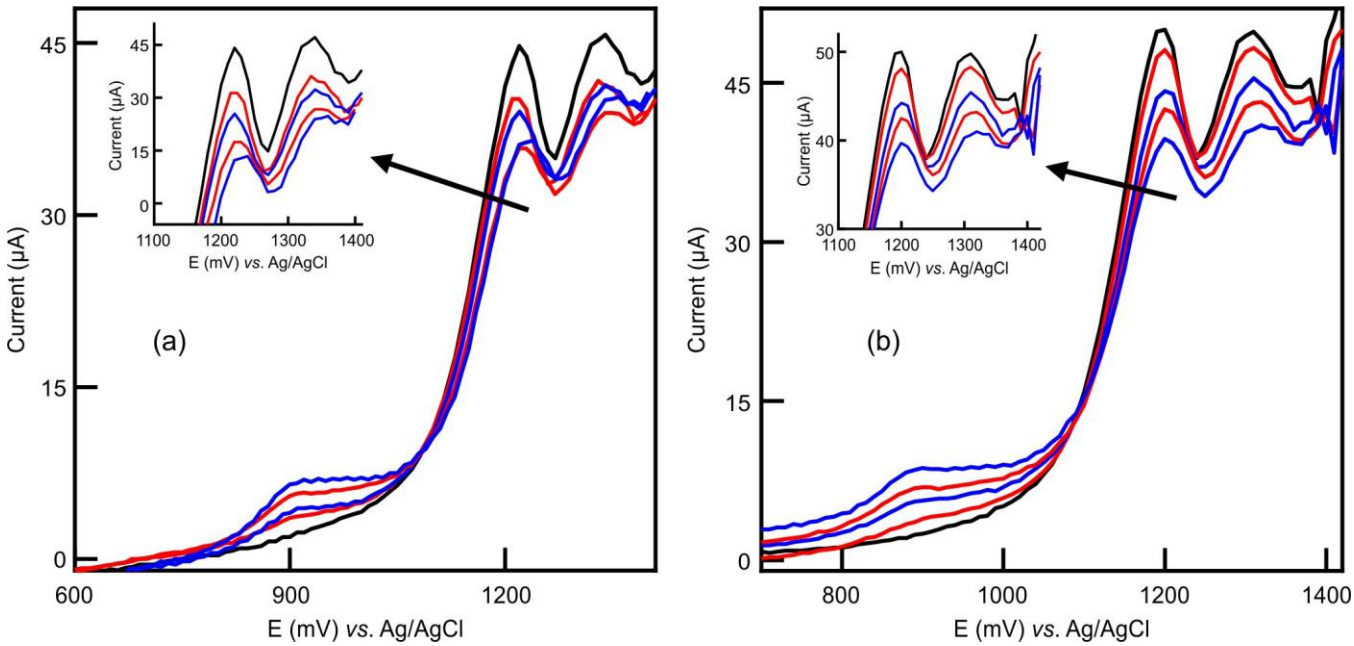

Fig. 11. AdS-SW voltammograms of 13 μM AVA at ABNPs/CPG-PE in PBS (pH 7.0) in presence of 0, 98, 196, 390, 778 nM DOX at (a) 25 ºC and (b) 37 ºC

Interaction of AVA with antihypertensive drug doxazosin: Clinical studies have shown that a significant decrease in blood pressure or an adverse event may occur when a PDE5 inhibitor is co-administered with an α1-adrenergic receptor blocker and carefulness must be taken. Consequently, it is crucial to investigate the interaction between the antihypertensive drug doxazosin (DOX), a selective α1-blocker and AVA to decide if there is a drug-drug interaction and to adjust AVA dosing if necessary. Therefore, the interaction between AVA and DOX was studied utilizing AdS-SWV with the designed ABNPs/CPG-PE sensor (Fig. 11). With the addition of various concentrations of DOX to the AVA solution, the height of the anodic peak current decreased and the peak potential shifted to a more positive value. These changes in both current and peak potential indicate an interaction between DOX and AVA. The obtained results show a new oxidation peak at 980 mV upon successive additions of DOX to the AVA solution (Fig. 11). The anodic peak corresponds to the electrooxidation of the amino group in the unbound DOX molecule [40]. The drug-drug interaction between AVA and DOX can be quantitatively assessed by determining the binding constant using the following equation (Fig. 12) [41]:

$$\mathrm{Log}\left(\frac{1}{\mathrm{DOX\,drug}}\right) = \mathrm{Log}\,(\mathrm{K}) + \mathrm{Log}\left(\frac{\mathrm{I_{H-G}}}{\mathrm{I_G} - \mathrm{I_{H-G}}}\right)$$

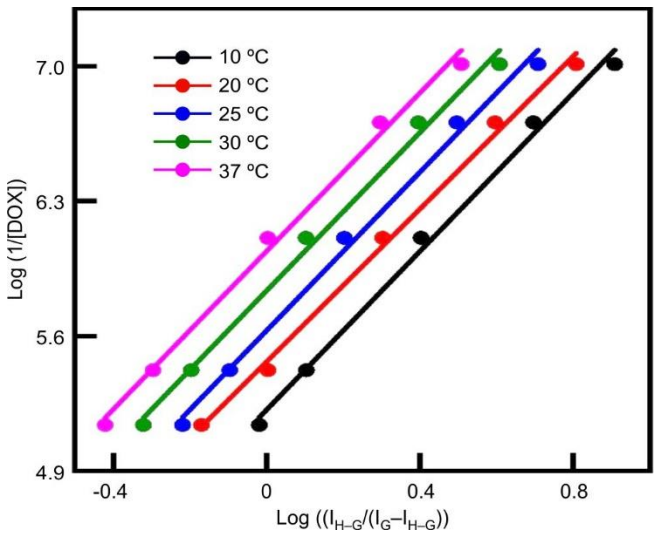

Fig. 12. Plots of log(1/[DOX]) *vs.* log($I_{H-G}/I_G–I_{H-G}$) illustrating the interaction between AVA and DOX at different temperatures

where K is the apparent binding constant, I_G and I_{H-G} are the peak currents of the unbound guest (G) and the complex formed between AVA and the DOX drug (H-G), respectively. The K values of this interaction were determined at different temperatures (Table-5), demonstrating stronger binding between

TABLE-5
BINDING CONSTANTS, STANDARD GIBBS FREE ENERGY, ENTHALPY AND ENTROPY CHANGES OF THE BINDING OF AVA WITH DOXAZOSIN

System	Temp. (ºC)	Log K	-ΔGº (kJ mol^{-1})	ΔHº (kJ mol^{-1})	ΔSº (J mol^{-1} K^{-1})
AVA–Doxazosin	10	5.22	28.27	51.955	282.8
	20	5.47	30.66		
	25	5.63	32.11		
	30	5.84	33.85		
	37	7.04	35.85		

the two drugs. It can be observed that the stability constants for the binding of AVA with DOX increase as the temperature rises from 10 ºC to 37 ºC. The most effective interaction between the two drugs occurs at the physiological temperature of 37 ºC. The obtained results suggest that a pharmacokinetic interaction between AVA and the antihypertensive drug DOX is expected. Therefore, adjusting the AVA dosage is essential when co-administered with DOX.

Thermodynamic studies of the interaction between AVA and DOX: To have a better insight into the interaction between AVA and DOX, thermodynamic parameters of the binding process were assessed. In this context, determining the binding constant at various temperatures provides a good means to indirectly calculate the enthalpy (ΔHº) and entropy (ΔSº) of the interaction process using the van't Hoff equation, as shown below [42]:

$$\ln K = -\frac{\Delta H^{o}}{RT} + \frac{\Delta S^{o}}{R}$$

The thermodynamic parameters (ΔHº and ΔSº) for the binding of AVA with DOX were derived from the linear behaviour of van't Hoff plots (ln K *versus* 1/T) (Table-5). These findings reveal that the interaction process of AVA with DOX is endothermic, indicated by a positive value for the ΔHº change. As well as the positive value of ΔSº displays an increase in the rotational and translational degrees of freedom in the drug-drug complex [43]. In this context, Ross & Subramanian [44] reported that when ΔHº > 0 and ΔSº > 0, hydrophobic interactions control the binding process. Therefore, the positive values of ΔHº and ΔSº suggest that the interaction of AVA and the DOX drug is primarily hydrophobic and the complexation process is entropy-controlled.

The change in Gibb's free energy is an important thermodynamic factor and its variation depends on the changes in ΔSº and ΔHº, as expressed in the following equation:

$$\Delta G^{o} = \Delta H^{o} - T\Delta S^{o}$$

The value of ΔGº for the interaction between AVA and DOX was also calculated using the standard thermodynamic equation:

$$\Delta G^{o} = -RT \ln K$$

The assessed values of ΔGº for the interaction of AVA and DOX are negative (Table-5), indicating that the binding process between the two drugs is thermodynamically spontaneous. Furthermore, the negative value of ΔGº increases with the rise in temperature, implying that the binding of AVA with DOX is more spontaneous at elevated temperatures. This result also supports the higher K values observed at higher temperatures. Considering the above results, the newly modified electrochemical sensor provides a new avenue to study drug-drug interactions, thereby preventing side effects.

Conclusion

The highlight of the present study is the development of a novel electrochemical device tailored for detecting Avanafil (AVA), an oral medication for the treatment of erectile dysfunction. This device is based on a composite pencil graphite paste electrode (CPG-PE) incorporated with acetylene black nanoparticles (ABNPs/CPG-PE) and it is used for detecting AVA in pharmaceutical products and human body fluids using AdS-SWV. The fabrication process of the new ABNPs/CPG-PE sensor is straightforward, efficient and cost-effective. SEM analysis revealed that the ABNPs/CPG-PE exhibited a surface with agglomerated features and white patches, confirming the modification of the CPG surface with ABNPs. The offered sensor exhibited superior performance, demonstrating high sensitivity, a wide linear range and lower LOD and LOQ, indicating its prominent electrochemical behaviour towards the oxidation of AVA. ABNPs-modified CPG-PE exhibited a low LOD (9.3×10^{-10} M) and broad linear range (0.002-1.96 μM and 1.96-19.6 μM) compared to other electrodes reported in the literature. The practical application of the constructed ABNPs/CPG-PE sensor achieved sensitivity, selectivity, cost-effectiveness and good recovery of AVA in human biological fluids and tablet dosage forms, eliminating the need for sample pretreatment before analysis. These findings pave the way for designing and fabricating other promising electrochemical sensors with high sensitivity for the trace determination of phosphodiesterase inhibitors in clinical patient blood. Furthermore, the interaction between AVA and doxorubicin (DOX) was studied utilizing AdS-SWV with the designed sensor ABNPs/CPG-PE. It was found that the most effective interaction between the investigated drugs occurs at the physiological temperature of 37 ºC. To gain better insight into drug-drug interactions, the thermodynamic characterisation of the binding process between AVA and DOX was assessed. It was concluded that AVA dose adjustment is necessary when co-administered with the antihypertensive drug DOX to avoid subsequent serious side effects in patients.

ACKNOWLEDGEMENTS

The authors extend their appreciation to Postgraduate Studies & Research Sector, Assiut University, which provided funding for materials procurement and analysis expenses (Project ID: AUN2025F.Sci.H0001). Special thanks to Prof. W. Schuhmann (Ruhr University, Bochum, Germany) for their valuable assistance in editing and refining the manuscript. One of the authors, Y. Temerk, is grateful to the Alexander von Humboldt-Stiftung, Germany for their support of this investigation.

CONFLICT OF INTEREST

The authors declare that there is no conflict of interests regarding the publication of this article.

DECLARATION OF AI-ASSISTED TECHNOLOGIES

During the preparation of this manuscript, the authors used an AI-assisted tool(s) to improve the language. The authors reviewed and edited the content and take full responsibility for the published work.

REFERENCES

1. N. Pyrgidis, I. Mykoniatis, A.B. Haidich, M. Tirta, D. Kalyvianakis, P. Talimtzi, A. Ouranidis and D. Hatzichristou, *Front. Pharmacol.*, **12**, 735708 (2021); https://doi.org/10.3389/fphar.2021.735708

2. C.N. McMahon, C.J. Smith and R. Shabsigh, *BMJ*, **332**, 589 (2006); https://doi.org/10.1136/bmj.332.7541.589
3. J.A. Kyle, D.A. Brown and J.K. Hill, *Ann. Pharmacother.*, **47**, 1312 (2013); https://doi.org/10.1177/1060028013501989
4. J. Kotera, H. Mochida, H. Inoue, T. Noto, K. Fujishige, T. Sasaki, T. Kobayashi, K. Kojima, S. Yee, Y. Yamada, K. Kikkawa and K. Omori, *J. Urol.*, **188**, 668 (2012); https://doi.org/10.1016/j.juro.2012.03.115
5. J. Krai, A. Beckenkamp, M. Gaelzer, A. Pohlmann, S. Guterres, E. Filippi-Chiela, C. Salbego, A. Buffon and R. Beck, *Biomed. Pharmacother.*, **94**, 10 (2017); https://doi.org/10.1016/j.biopha.2017.07.048
6. J. Jung, S. Choi, S.H. Cho, J.L. Ghim, A. Hwang, U. Kim, B.S. Kim, A. Koguchi, S. Miyoshi, H. Okabe, K.S. Bae and H.-S. Lim, *Clin. Ther.*, **32**, 1178 (2010); https://doi.org/10.1016/j.clinthera.2010.06.011
7. K.A.M. Attia, A.A. Mohamad, M.S. Emara, A.M. Abdel-Raoof, M.A. Hasan, A.W. Madkour and E.A. El-Desouky, *RSC Adv.*, **11**, 3834 (2021); https://doi.org/10.1039/D0RA08216C
8. T.A. Mohamed and S.A. Atty, *Spectrochim. Acta A Mol. Biomol. Spectrosc.*, **229**, 117898 (2020); https://doi.org/10.1016/j.saa.2019.117898
9. M.N. Patel and C.S. Kothari, *J. AOAC Int.*, **99**, 649 (2016); https://doi.org/10.5740/jaoacint.15-0259
10. M.K. Darwish, M.M. Soliman and S.A. Abdel-Razeq, *Asian J. Chem. Sci.*, **6**, 1 (2019).
11. A.K. Kammoun, A. Khedr and O.A.A. Ahmed, *RSC Adv.*, **10**, 9407 (2020); https://doi.org/10.1039/D0RA00569J
12. N.Ö. Can, *Molecules*, **23**, 1771 (2018); https://doi.org/10.3390/molecules23071771
13. M.B. Ali, A.M. Abdel-Raoof, H.A.M. Hendawy, W. Talaat, G.A. Omran and S. Morshedy, *J. Electrochem. Soc.*, **168**, 087510 (2021); https://doi.org/10.1149/1945-7111/ac1d7d
14. A.M.B.H. Ali, F.A.M. Abdel-aal, A.H. Rageh and A.M.I. Mohamed, *Microchem. J.*, **172**, 106895 (2022); https://doi.org/10.1016/j.microc.2021.106895
15. M.B.H. Ali, A.H. Rageh, F.A.M. Abdel-aal and A.M.I. Mohamed, *Microchem. J.*, **185**, 108261 (2023); https://doi.org/10.1016/j.microc.2022.108261
16. H.M. Ali, I. Hotan Alsohaimi, A.A. Nayl, A.A. Essawy, M. Gamal and H. Ibrahim, *Microchem. J.*, **183**, 108068 (2022); https://doi.org/10.1016/j.microc.2022.108068
17. H.M. Ali, I.A. Alhagri and H. Ibrahim, *J. Electroanal. Chem.*, **907**, 116067 (2022); https://doi.org/10.1016/j.jelechem.2022.116067
18. H. Ibrahim and Y. Temerk, *Microchem. J.*, **178**, 107425 (2022); https://doi.org/10.1016/j.microc.2022.107425
19. M. Ibrahim, Y. Temerk and H. Ibrahim, *RSC Adv.*, **7**, 32357 (2017); https://doi.org/10.1039/C7RA04331G
20. H. Ibrahim and Y. Temerk, *Talanta*, **208**, 120362 (2020); https://doi.org/10.1016/j.talanta.2019.120362
21. Y. Temerk and H. Ibrahim, *J. Electroanal. Chem.*, **782**, 9 (2016); https://doi.org/10.1016/j.jelechem.2016.09.042
22. M.A. Rashed, M. Faisal, F.A. Harraz, M. Jalalah, M. Alsaiari and S.A. Alsareii, *J. Electrochem. Soc.*, **168**, 027512 (2021); https://doi.org/10.1149/1945-7111/abe44b
23. W. Meng, W. Zhang, J. Zhang, X. Chen and Y. Zhang, *Anal. Methods*, **11**, 2183 (2019); https://doi.org/10.1039/C9AY00064J
24. M. Ibrahim, H. Ibrahim, N.B. Almandil, M.A. Sayed and A.N. Kawde, *Anal. Methods*, **12**, 2846 (2020); https://doi.org/10.1039/D0AY00507J
25. M. Ibrahim, Y. Temerk, H. Ibrahim and M. Salah, *Chin. J. Anal. Chem.*, **52**, 100418 (2024); https://doi.org/10.1016/j.cjac.2024.100418
26. H. Ibrahim and Y. Temerk, *Sens. Actuators B Chem.*, **347**, 130626 (2021); https://doi.org/10.1016/j.snb.2021.130626
27. R. da Silva, P. Cervini, R.M. Buoro and E.T.G. Cavalheiro, *Mater. Today Commun.*, **31**, 103691 (2022); https://doi.org/10.1016/j.mtcomm.2022.103691
28. R. da Silva, L.G. da Silva Catunda and R.M. Buoro, *J. Solid State Electrochem.*, **28**, 3999 (2024); https://doi.org/10.1007/s10008-024-06012-3
29. W. Huang, W. Qu and D. Zhu, *Bull. Korean Chem. Soc.*, **29**, 1323 (2008); https://doi.org/10.5012/bkcs.2008.29.7.1323
30. D. Sun and H. Zhang, *Anal. Chim. Acta*, **557**, 64 (2006); https://doi.org/10.1016/j.aca.2005.10.002
31. X. Yang and H. Zhang, *Food Chem.*, **102**, 1223 (2007); https://doi.org/10.1016/j.foodchem.2006.07.010
32. M. Ibrahim, H. Ibrahim, N.B. Almandil and A.-N. Kawde, *J. Electroanal. Chem.*, **824**, 22 (2018); https://doi.org/10.1016/j.jelechem.2018.07.031
33. G. Li, Z. Ji and K. Wu, *Anal. Chim. Acta*, **577**, 178 (2006); https://doi.org/10.1016/j.aca.2006.06.061
34. H.L. Lord, W. Zhan and J. Pawliszyn, *Anal. Chim. Acta*, **677**, 3 (2010); https://doi.org/10.1016/j.aca.2010.06.020
35. E. Er, H. Çelikkan, N. Erk and M.L. Aksu, *Electrochim. Acta*, **157**, 252 (2015); https://doi.org/10.1016/j.electacta.2015.01.020
36. A. Pourhabib and M. Arvand, *J. Anal. Chem.*, **77**, 235 (2022); https://doi.org/10.1134/S1061934822020022
37. N.S. Prinith, J.G. Manjunatha, M.D. Albaqami, A.M. Tighezza and M. Sillanpää, *ChemistrySelect*, **7**, e202203572 (2022); https://doi.org/10.1002/slct.202203572
38. E. Laviron, *J. Electroanal. Chem. Interfacial Electrochem.*, **101**, 19 (1979); https://doi.org/10.1016/S0022-0728(79)80075-3
39. M.I.C. Marinho, M.F. Cabral and L.H. Mazo, *J. Electroanal. Chem.*, **685**, 8 (2012); https://doi.org/10.1016/j.jelechem.2012.08.023
40. A. Arranz, J.M. Moreda and J.F. Arranz, *Mikrochim. Acta*, **134**, 69 (2000); https://doi.org/10.1007/s006040070056
41. Y. Temerk, M. Ibrahim, H. Ibrahim and W. Schuhmann, *RSC Advances*, **8**, 25387 (2018); https://doi.org/10.1039/C8RA03231A
42. S. Tommasini, D. Raneri, R. Ficarra, M.L. Calabrò, R. Stancanelli and P. Ficarra, *J. Pharm. Biomed. Anal.*, **35**, 379 (2004); https://doi.org/10.1016/S0731-7085(03)00647-2
43. Y.M. Temerk, M.S. Ibrahim and M. Kotb, *Spectrochim. Acta A Mol. Biomol. Spectrosc.*, **71**, 1830 (2009); https://doi.org/10.1016/j.saa.2008.07.001
44. P.D. Ross and S. Subramanian, *Biochemistry*, **20**, 3096 (1981); https://doi.org/10.1021/bi00514a017